

# Centrally Peaked X-Ray Supernova Remnants in the Small Magellanic Cloud Studied with ASCA and ROSAT

Jun YOKOGAWA, Kensuke IMANISHI, Katsuji KOYAMA

*Department of Physics, Graduate School of Science, Kyoto University, Sakyo-ku, Kyoto 606-8502*

*jun@cr.scphys.kyoto-u.ac.jp*

*kensuke@cr.scphys.kyoto-u.ac.jp*

*koyama@cr.scphys.kyoto-u.ac.jp*

Mamiko NISHIUCHI

*Japan Atomic Energy Research Institute, Kansai Research Establishment,*

*8-1 Umebi-dai, Kizu-cho, Soraku-gun, Kyoto 619-0215*

*nishiuchi@apr.jaeri.go.jp*

and

Norikazu MIZUNO

*Department of Astrophysics, Nagoya University, Furo-cho, Chikusa-ku, Nagoya 464-8602*

*norikazu@astrophys.nagoya-u.ac.jp*

(Received 2001 June 18; accepted 2001 December 27)

## Abstract

This paper presents ASCA/SIS and ROSAT/HRI results of three supernova remnants (SNRs) in the Small Magellanic Cloud: 0103–726, 0045–734, and 0057–7226. The ROSAT/HRI images of these SNRs indicate that the most of the X-ray emissions are concentrated in the center region. Only from 0103–726 are faint X-rays along the radio shell also detected. The ASCA/SIS spectra of 0103–726 and 0045–734 exhibit strong emission lines from highly ionized metals. The spectra were well-fitted with non-equilibrium ionization (NEI) plasma models. The metal abundances are found to be larger than the mean chemical compositions in the interstellar medium (ISM) of the SMC. Thus, X-rays from these two SNRs are attributable to the ejecta gas, although the ages estimated from the ionization timescale are significantly large,  $\gtrsim 10^4$  yr. The chemical compositions are roughly consistent with the type-II supernova origin of a progenitor mass  $\lesssim 20M_{\odot}$ . The SIS spectrum of 0057–7226 was also fitted with an NEI model of an estimated age  $\gtrsim 6 \times 10^3$  yr. Although no constraint on the metal abundances was obtained, the rather weak emission lines are consistent with the low metal abundances in the ISM of the SMC. A possible scenario for the evolution of the morphologies and spectra of SNRs is proposed.

**Key words:** H II regions — ISM: abundances — ISM: individual (0103–726, 0045–734, 0057–7226) — Magellanic Clouds — supernova remnants — X-rays: ISM

## 1. Introduction

The Large and Small Magellanic Clouds (hereafter LMC and SMC) are ideal galaxies for systematic X-ray studies of SNRs, because of their reasonable sizes, well-calibrated distances (50 kpc and 60 kpc, respectively; 000 [cite]cite.ber2000van den Bergh(2000)), and low interstellar absorptions.

[cite]cite.wil1999Williams et al.(1999) ([cite]cite.wil1999Williams et al.(1999)) obtained X-ray images of LMC SNRs mainly with ROSAT/HRI, and classified the SNRs into six classes according to the morphology. They found a loose correlation between the SNR sizes and the morphological classes: the smaller SNRs tend to exhibit shell-like X-ray emission, while the larger ones have “diffuse-face” or centrally-brightened morphologies. This correlation indicates the evolution from shell-like to centrally-brightened SNRs. [cite]cite.wil1999Williams

et al.(1999) ([cite]cite.wil1999Williams et al.(1999)) argued that the centrally brightened morphologies could be produced by the cloud evaporation model (000 [cite]cite.whi1991White, Long(1991)) or the fossil radiation model (000 [cite]cite.rho1998Rho, Petre(1998), and references therein).

[cite]cite.hug1998Hughes et al.(1998) ([cite]cite.hug1998Hughes et al.(1998)) systematically studied the ASCA/SIS spectra of seven middle-aged SNRs with a model assuming an internal structure based on the Sedov solution. They found that the average metal abundances in the SNRs decrease with increasing SNR age, and gradually approach to the mean value of the interstellar medium (ISM) in the LMC. [cite]cite.nis2001Nishiuchi(2001) ([cite]cite.nis2001Nishiuchi(2001)) analyzed nine fainter LMC SNRs in a less-systematic way and determined the basic plasma parameters. Besides the general tendency of the abundance decrease, five SNRs among the 16 SNRs examined by [cite]cite.hug1998Hughes

et al.(1998) ([cite]cite.hug1998Hughes et al.(1998)) and te]cite.nis2001Nishiuchi(2001) ([cite]cite.nis2001Nishiuchi(2001)) show overabundances of several elements (overabundant species are different for each SNR).

In the SMC, on the other hand, detailed X-ray studies have been limited to the brightest and youngest SNR, 0102–723, due mainly to the far-fainter X-rays from the other SNRs. te]cite.hay1994Hayashi et al.(1994) ([cite]cite.hay1994Hayashi et al.(1994)) analyzed the ASCA/SIS spectrum from the full region of 0102–723 and found overabundances of heavy elements, consistent with a type-II young SNR. With the Chandra ACIS, te]cite.hug2000Hughes et al.(2000) ([cite]cite.hug2000Hughes et al.(2000)) have spatially resolved X-rays from the blast-wave and those from the ejecta-dominated inner region; the former exhibits low elemental abundances consistent with the SMC ISM, while the latter is overabundant, especially in O and Ne.

The second-brightest X-ray SNR in the SMC is 0103–726, and the next luminous class includes several SNRs, such as 0045–734 and 0057–7226 (000 [cite]cite.hab2000Haberl et al.(2000)). All of these SNRs are located in H II regions, DEM S125, N19, and N66, respectively (e.g., 000 [cite]cite.fil1998Filipović et al.(1998)). te]cite.mil1982Mills et al.(1982) ([cite]cite.mil1982Mills et al.(1982)) carried out radio observations with the Molonglo Observatory synthesis telescope (MOST) and determined the diameters of the former two SNRs to be  $\sim 52$  pc (0103–726) and  $\sim 25$  pc (0045–734). The Einstein/HRI image of 0103–726 shows extended X-rays with the same size of radio emission (000 [cite]cite.ino1983Inoue et al.(1983)).

In order to distinguish SNRs from the strong background emission of the H II region, te]cite.ye1991Ye et al.(1991) ([cite]cite.ye1991Ye et al.(1991)) made a map of the intensity difference between  $H\alpha$  and the radio continuum, instead of the conventional method of using the intensity ratio of  $[S II]/H\alpha$ . They then found a non-thermal shell structure with a diameter of  $\sim 56$  pc, the SNR 0057–7226, from the most luminous H II region in the SMC, N66. The sizes of these three SNRs are thus much larger than that of 0102–723,  $\sim 8$  pc (000 [cite]cite.mil1982Mills et al.(1982)). By an analogy of the LMC samples used by te]cite.hug1998Hughes et al.(1998) ([cite]cite.hug1998Hughes et al.(1998)), these large sizes indicate that the three SNRs should be very old, possibly older than  $10^4$  yr, or even more. In fact, te]cite.ros1994Rosado et al.(1994) ([cite]cite.ros1994Rosado et al.(1994)) carried out a kinematic study in  $H\alpha$  emission and determined an age of 0045–734 to be  $5.7 \times 10^4$  yr with a Sedov phase assumption. Usually, X-ray spectra from such large (old) SNRs are expected to exhibit low metal abundances consistent with the ISM, as has already been reported in the LMC samples (000 [cite]cite.hug1998Hughes et al.(1998)).

However, a preliminary analysis of the ASCA spectra by te]cite.yok2000Yokogawa et al.(2000) ([cite]cite.yok2000Yokogawa et al.(2000)) does not agree with the above prediction, except for

0057–7226 (N66): overabundances of several elements suggested for 0103–726 and 0045–734 (N19). We therefore carried out more detailed and elaborate X-ray studies on the three SNRs with a uniform analysis, using the high-resolution spectroscopy and imaging data of the ASCA/SIS and ROSAT/HRI, as well as information from radio observations.

## 2. Observations and Data Reduction

ASCA observations of 0103–726, 0045–734, and 0057–7226 were carried out with two GISs (Gas Imaging Spectrometers, 000 [cite]cite.oha1996Ohashi et al.(1996)) and two SISs (Solid-state Imaging Spectrometers, 000 [cite]cite.bur1994Burke et al.(1994)) on the focal planes of the four XRTs (X-ray Telescopes, 000 [cite]cite.ser1995Serlemitsos et al.(1995)). To study the spectra, we used only the SIS data, which had better energy resolution ( $\sim 2\%$  at 5.9 keV) than the GIS; hence, we do not refer to the GIS in this paper. The date and SIS operation mode of each observation are listed in table 1.

We rejected the SIS data obtained in the South Atlantic Anomaly, in low cut-off rigidity regions ( $< 4$  GV), when the elevation angle was low ( $< 5^\circ$ ), or when the elevation from the bright earth was low ( $< 25^\circ$ ). Hot and/or flickering pixels were also removed. In order to restore the quality degradation after long-year operation in orbit, we applied a correction of the Residual Dark Distribution (T. Dotani et al. 1997, ASCA News 5, 14), which is available only for faint-mode data. After these screenings, the total available exposure times were  $\sim 61$  ks for 0103–726,  $\sim 134$  ks for 0045–734, and  $\sim 34$  ks for 0057–7226 (see table 1).

Since the spatial resolution of ASCA is limited ( $\sim 3'$  in a half-power diameter), we used ROSAT/HRI data (resolution is  $\sim 6''$ ) for an imaging study. We retrieved screened image data of 0103–726, 0045–734, and 0057–7226, for which the sequence IDs are rh500428, rh500136, and rh900445, respectively, from the HEASARC Online Service. The observation of each SNR was made by two or three separate exposures centered on the same coordinates. We combined the data from those exposures, resulting in total available exposure times of  $\sim 31$  ks for 0103–726,  $\sim 12$  ks for 0045–734, and  $\sim 49$  ks for 0057–7226 (see table 1).

## 3. Analyses and Results

### 3.1. ROSAT HRI Images

The X-ray images obtained with ROSAT/HRI are shown and compared with the radio continuum emission in figure 1. Radio images at 843 MHz, obtained with MOST (000 [cite]cite.mil1982Mills et al.(1982)), are overlaid for (a) 0103–726 and (b) 0045–734. For 0057–7226, the difference map of  $H\alpha$  and the MOST images, which selectively reveals non-thermal radio emission (000 [cite]cite.ye1991Ye et al.(1991)), are overlaid in (c).

The radio emission of 0103–726 has a faint shell with

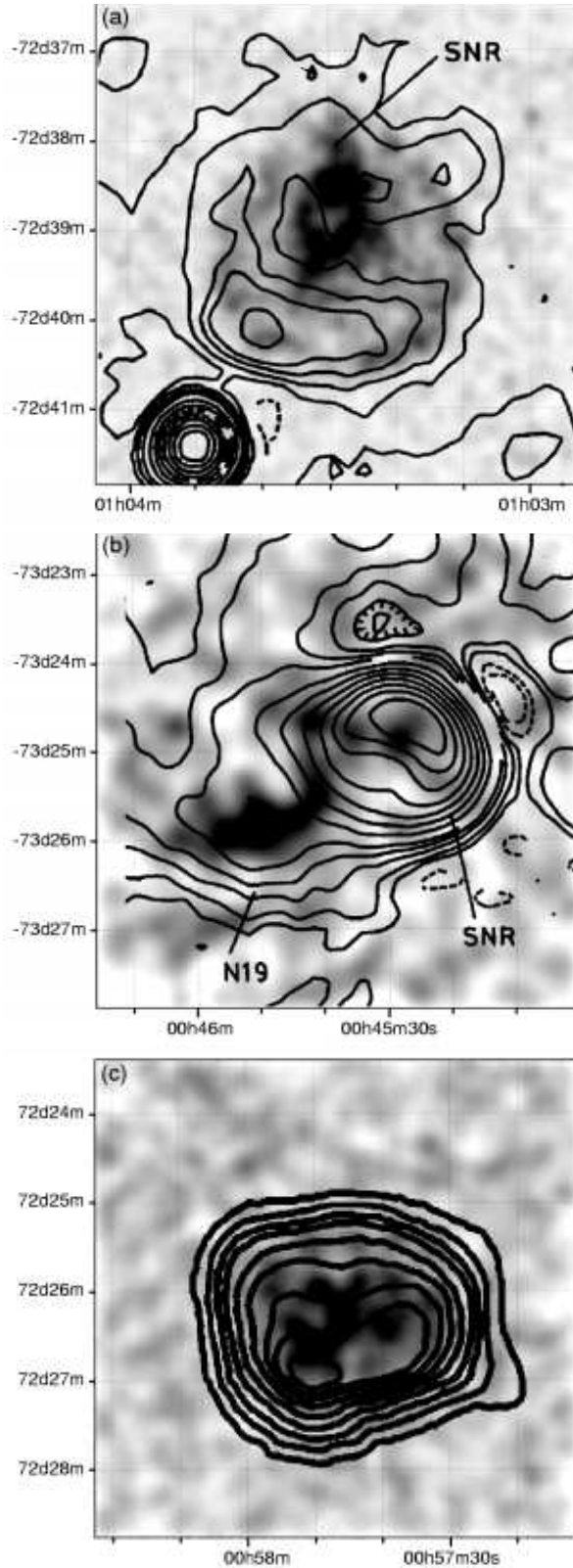


**Fig. 1.** Gray-scale X-ray images of (a) 0103–726, (b) 0045–734, and (c) 0057–7226, obtained with ROSAT/HRI. Overlaid contours are (a,b) the MOST radio image at 843 MHz taken from [te\[cite\]cite.mil1982Mills et al.\(1982\)](#) ([\[cite\]cite.mil1982Mills et al.\(1982\)](#)), (c) the difference map of H $\alpha$  and MOST 843 MHz images reproduced from [te\[cite\]cite.ye1991Ye et al.\(1991\)](#) ([\[cite\]cite.ye1991Ye et al.\(1991\)](#)). The equinox of the equatorial coordinates is 1950.0. Strong radio emission at the southeast of 0103–726 is a background point source.

an  $\sim 3'$  diameter, in addition to enhanced emission at the southwest (SE) part. The X-rays show a faint shell with an  $\sim 2.5'$  diameter along the radio shell, which was already noted in an earlier result (000 [\[cite\]cite.ino1983Inoue et al.\(1983\)](#)). More prominent X-rays are found near the center of the radio shell with a small offset of  $\sim 30''$  to the north. These central X-rays exhibit a small elliptical ring.

The radio emission from 0045–734 is extended to  $\sim 3' \times 4'$ , with a partial shell at the northwest (NW) and a weak diffuse structure to the SE. The NW shell exhibits strong [S II] optical lines, while several weak [S II] filaments are found within the SE emission (000 [\[cite\]cite.mat1983Mathewson et al.\(1983\)](#)). No shell-like structure is found in the X-ray band. Instead, the X-ray emission exhibits an irregular shape with strong emission at SE and faint knots at NW, both of which are confined to within the radio shell and diffuse structure. According to [te\[cite\]cite.dic2001Dickel et al.\(2001\)](#) ([\[cite\]cite.dic2001Dickel et al.\(2001\)](#)), the west-most knot may correspond to another SNR candidate, MCRX J0047.2–7308. However, this knot is much fainter than the remaining part of the X-ray emission, and hence contamination from MCRX J0047.2–7308 would be small. Therefore, the following results would fairly well represent the properties of 0045–734.

The non-thermal radio emission from 0057–7226 exhibits a shell-like structure with a diameter of  $\sim 3'$ , while the X-rays are concentrated in the radio shell, with a diameter of  $\sim 2'$ .

### 3.2. ASCA SIS Spectra

We extracted the source spectra from the entire regions of each SNR, while the background spectra were taken from nearby source-free regions. The spectra from SIS-0 and SIS-1 were co-added so as to increase the statistics. The background-subtracted spectra are shown in figure 2. Since the spectra of these SNRs show emission lines from highly ionized heavy elements (000 [\[cite\]cite.yok2000Yokogawa et al.\(2000\)](#)), we fitted the spectra with an optically thin thermal-plasma model in a non-equilibrium ionization (NEI) state, coded by [te\[cite\]cite.mas1994Masai\(1994\)](#) ([\[cite\]cite.mas1994Masai\(1994\)](#)). The physical parameters in the NEI model are the electron temperature ( $kT_e$ ), the metal abundances, and the ionization timescale,  $\tau = n_e t$ , where  $n_e$  is the electron density and  $t$  is the elapsed time after the plasma was heated up.

We first fitted the spectrum of 0103–726 with a fixed abundance of 0.2 solar, which is the mean value of the ISM of the SMC (000 [\[cite\]cite.rus1992Russell, Dopita\(1992\)](#); hereafter, “SMC mean value”). This model, however, left bump-like (line-like) residuals at the energies of the K-shell emission lines from O, Ne, Mg, and Si, and Fe-L. Therefore, we allowed abundances of O, Mg, and Si to vary freely. In addition, since the Ne-K and Fe-L lines may equally contribute to X-ray emission around  $\sim 1$  keV, we treated the abundances of Ne and Fe according to the following three cases: (I) Ne is free, (II) Fe is free, and (III) both Ne and Fe are free. Model II, however, was

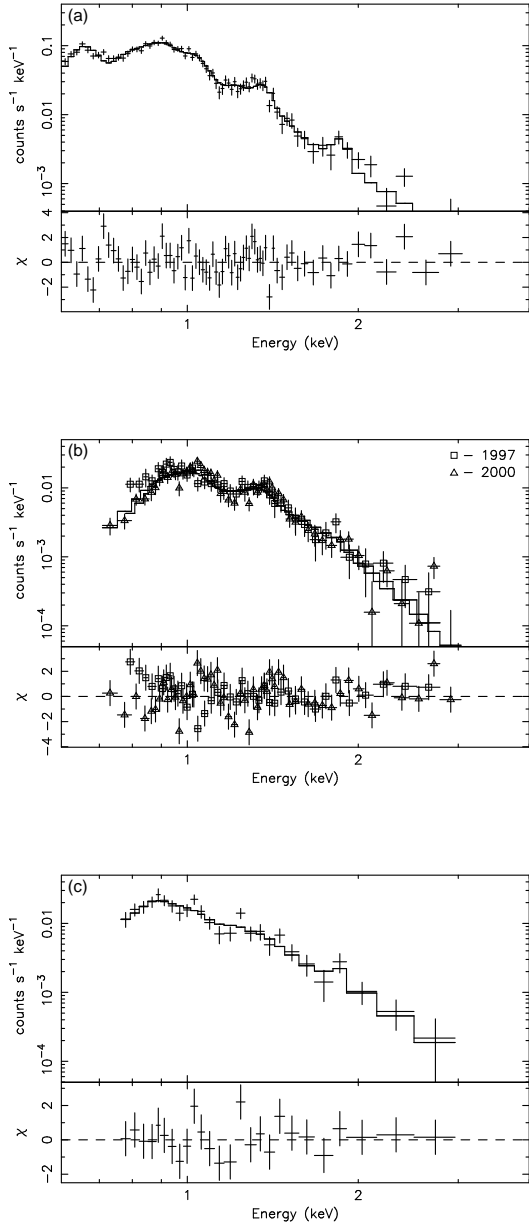


**Fig. 2.** X-ray spectra of (a) 0103–726, (b) 0045–734, and (c) 0057–7226, obtained with ASCA SIS-0+SIS-1. The crosses and the solid lines in each top panel indicate the data points and the best-fit models (model III for 0103–726 and model I for 0045–734; see table 2), respectively. The bottom panels show the residuals from the best-fit models. The squares and triangles in (b) represent the observations in 1997 and 2000, respectively.

rejected with  $\chi^2 = 124$  for 64 degrees of freedom (d.o.f.), while models I and III gave much better fits ( $\chi^2$  is 94.1 and 88.8, respectively). Even these two models were rejected from a statistical point of view, possibly due to the residual uncertainty of the response function after the RDD correction. To extract a more accurate response is impractical at this moment; thus, we adopt these models

in the following discussion as a reasonable approximation. The best-fit parameters for models I and III are given in table 2. In both models, the heavy elements show larger abundances than the SMC mean value.

For 0045–734, the spectra from the two separate observations were simultaneously fitted (all of the free parameters were linked between the two spectra). We first fitted the spectra with an NEI model of fixed abundances to the SMC mean value. Since the residuals remained at energies of emission lines from Ne-K/Fe-L and Mg-K, we fit the spectra with an NEI model in which the abundance of Mg was a free parameter, and those of Ne and Fe were treated as described above (models I–III). For model III, the best-fit temperature is extremely large,  $kT_e \sim 25$  keV. Such a high temperature would be unphysical because youngest SNRs ever known exhibit a much lower temperature (several keV). We thus do not adopt model III. Models I and II, on the other hand, gave equally better fits with no bump-like (line-like) residuals. For the same reason described above, we adopt these models hereafter. The best-fit parameters of models I and II are given in table 2. In both models, the abundances of Mg and Ne/Fe are larger than those of the SMC mean value.

Although the spectrum of 0057–7226 was well-fitted with an NEI model with free-abundances, we could not constrain the abundances due to the limited statistics. We hence fixed the abundances to be 0.2 solar (the SMC mean value). The best-fit parameters are given in table 2.

## 4. Discussion

### 4.1. Plasma Parameters in the SNRs

Using the X-ray images (figure 1), we estimated the volume  $V$  of the X-ray emitting plasma. For simplicity, we assumed that the plasma in 0103–726 and 0057–7226 fills a sphere with a diameter of  $2'5$  and  $2'$ , respectively, while that in 0045–734 fills a cylinder with a height of  $3'$  and a diameter of  $1'$ . We then obtained  $V = 1.3 \times 10^{60} \cdot \beta \text{ cm}^3$  for 0103–726,  $V = 3.6 \times 10^{59} \cdot \beta \text{ cm}^3$  for 0045–734, and  $V = 6.6 \times 10^{59} \cdot \beta \text{ cm}^3$  for 0057–7226, respectively, where  $\beta$  represents the volume filling factor, which could be different for each SNR.

From the emission measure  $EM$  determined by the spectral fitting, we could estimate the electron density of the plasma,  $n_e$ , by  $n_e = \sqrt{EM/V}$ . The number density of the nucleons was simply assumed to be the same as that of electrons. The age  $t$  was then determined from the ionization timescale,  $\tau$ , by  $t = \tau/n_e$ . The total mass of the plasma  $M_{\text{total}}$  was estimated by  $M_{\text{total}} = n_e V m_H$ , where  $m_H$  is the mass of a hydrogen atom. We then determined the mass of the overabundant heavy elements, using  $M_{\text{total}}$  and the best-fit abundances. These estimated parameters are given in table 3. The lower limit for the ionization age of 0045–734 is  $2.9 \times 10^4$  yr in both models, which is consistent with the age of  $5.7 \times 10^4$  yr derived from an optical study of the kinematics (000 [cite]cite.ros1994Rosado et al.(1994)).

For 0103–726 and 0045–734, the abundances are significantly larger than the SMC mean value in any model;

hence, the ejecta should largely contribute to the X-ray emitting plasma. In figure 3, we compare the estimated element masses for 0103–726 and 0045–734 with the theoretical predictions of chemical compositions produced with supernovae (SNe) from various progenitor masses (000 [cite]cite.tsu1995Tsujiimoto et al.(1995)). Type-Ia origin would be rejected for both of the SNRs, because the data largely exceed the theoretical prediction for Ne and Mg, while the data do not show a large excess of Fe, as expected from theory. On the other hand, our data roughly agree with the prediction for a type-II SN case with a progenitor mass of  $\lesssim 20M_{\odot}$ . Since these SNRs are located in H II regions, the type-II SNe origin is reasonable.

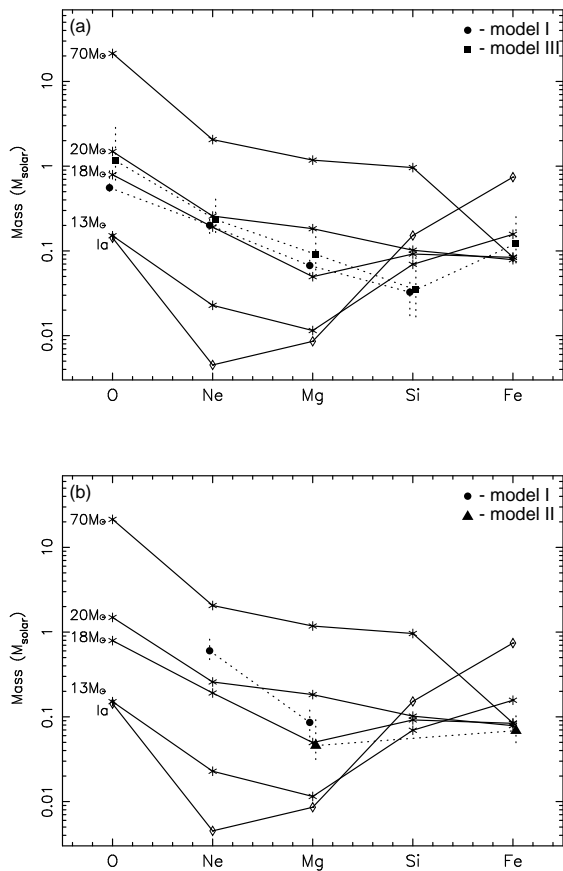


**Fig. 3.** Nucleosynthesis products of various SNe overlaid with the masses of elements in (a) 0103–726 and (b) 0045–734 derived from the spectral analyses. Solid lines with asterisks and diamonds represent products in type-II and type-Ia SNe, respectively (000 [cite]cite.tsu1995Tsujiimoto et al.(1995)). The progenitor masses of the type-II SNe are also indicated. The dotted lines with circles, triangles, and squares represent models I, II, and III, respectively. Model II for 0103–726 and model III for 0045–734 are not plotted because of the bad fitting (see subsection 3.2). Plots for the elements fixed to be 0.2 solar in the fitting are not presented.

The spectrum of 0057–7226 does not exhibit overabundances, and is consistent with the SMC ISM. Therefore,

the type of the SN cannot be constrained. However, its location in a giant H II region prefers a type-II origin.

Since the total mass of the “metal-poor” SNR 0057–7226 is comparable to those of “metal-rich” SNRs 0103–726 and 0045–734, 0057–7226 may simply have a smaller ejecta mass than the other two SNRs. One may argue, alternatively, if the progenitor is less massive than those of 0103–726 and 0045–734, for example  $\sim 13M_{\odot}$ , that the abundances of O, Ne, and Mg may be explained (see solid lines in figure 3). However, this model predicts a larger mass of Fe, which is not found in the observed spectrum.

#### 4.2. Implication for the SNR Evolution

We have shown that the X-ray emissions of the three SNRs are predominantly concentrated inside the radio shells (hereafter, “centrally peaked” morphology). The X-ray spectra predict that the ages are all rather old ( $\gtrsim 10^4$  yr), while two of them are found to exhibit high abundances possibly due to the ejecta gas.

To explain these features as well as the results from the LMC SNRs (000 [cite]cite.wil1999Williams et al.(1999); 000 [cite]cite.hug1998Hughes et al.(1998); 000 [cite]cite.nis2001Nishiuchi(2001)), we propose the following scenario. Soon after an SNR enters the Sedov phase (i.e., middle-aged stage), X-ray emission from the swept-up ISM becomes dominant because of the higher density at the shell, and hence the SNR exhibits a shell-like morphology and a low-abundance spectrum. As the age increases, the abundances gradually decrease and approach the mean value of the ISM, due to dilution with the swept-up ISM. At the same time, the morphology gradually changes from shell-like (“Shell” and “Diffuse Face 1” in 000 [cite]cite.wil1999Williams et al.(1999)) to centrally-peaked type (“Diffuse Face 2” and “Centrally Brightened” in 000 [cite]cite.wil1999Williams et al.(1999)), due to rapid cooling of the shell compared with the inner region. X-rays from the central region may thus be fossil radiation (000 [cite]cite.rho1998Rho, Petre(1998), and references therein) and could be enhanced by the evaporation of cloudlets (000 [cite]cite.whi1991White, Long(1991)). The X-ray-emitting plasma shows a scatter of metal abundances, depending on the ejecta mass (large ejecta mass for 0103–726 and 0045–734 and small ejecta mass for 0057–7226). This scenario would be supported by numerical simulations by [cite]cite.she1999Shelton(1999) ([cite]cite.she1999Shelton(1999)).

The middle-aged LMC SNRs analyzed by [cite]cite.hug1998Hughes et al.(1998) ([cite]cite.hug1998Hughes et al.(1998)) and [cite]cite.nis2001Nishiuchi(2001) ([cite]cite.nis2001Nishiuchi(2001)) contain five shell-like and seven centrally-peaked SNRs (000 [cite]cite.wil1999Williams et al.(1999)); among them, one shell-like and three centrally-peaked SNRs were found to be overabundant. The fact that the ratio of the overabundant SNRs is higher for the centrally-peaked (3/7) than for the shell-like (1/5) may support the above scenario, although the statistics are still limited.

In a transition phase from a shell-like to a centrally-

peaked SNR, a faint X-ray shell, like that of 0103–726, may be observed. In this case, the X-ray spectrum of the faint shell should exhibit low abundances consistent with the SMC ISM, while the inner part should exhibit an ejecta-dominated spectrum. Spatially resolved spectroscopy with Chandra or XMM-Newton should clarify this prediction.

The authors are grateful to Dr. K. Yoshita, whose strong criticism and useful comments made the initial draft much better. The authors also thank constructive comments from the referee, Dr. R. Williams. J.Y. and K.I. are supported by the JSPS Research Fellowship for Young Scientists. We retrieved ROSAT data from the HEASARC Online System which is provided by NASA/GSFC.

## References

- [Burke et al.(1994)] Burke, B. E., Mountain, R. W., Daniels, P. J., Dolat, V. S., & Cooper, M. J. 1994, *IEEE Trans. Nucl. Sci.*, 41, 375
- [Dickel et al.(2001)] Dickel, J. R., Williams, R. M., Carter, L. M., Milne, D. K., Petre, R., & Amy, S. W. 2001, *AJ* 122, 849
- [Filipović et al.(1998)] Filipović, M. D., Pietsch, W., Haynes, R. F., White, G. L., Jones, P. A., Wielebinski, R., Klein, U., Dennerl, K., Kahabka, P., & Lazendic, J. S. 1998, *A&AS*, 127, 119
- [Haberl et al.(2000)] Haberl, F., Filipović, M. D., Pietsch, W., & Kahabka, P. 2000, *A&AS*, 142, 41
- [Hayashi et al.(1994)] Hayashi, I., Koyama, K., Ozaki, M., Miyata, E., Tsunemi, H., Hughes, J. P., & Petre, R. 1994, *PASJ*, 46, L121
- [Hughes et al.(1998)] Hughes, J. P., Hayashi, I., & Koyama, K. 1998, *ApJ*, 505, 732
- [Hughes et al.(2000)] Hughes, J. P., Rakowski, C. E., & Decourchelle, A. 2000, *ApJ*, 543, L61
- [Inoue et al.(1983)] Inoue, H., Koyama, K., & Tanaka, Y. 1983, in *IAU Symp. 101, Supernova remnants and their X-ray emission*: ed. J. Danziger & P. Gorenstein (Dordrecht: D. Reidel Pub. Co.), p.535
- [Masai(1994)] Masai, K. 1994, *ApJ*, 437, 770
- [Mathewson et al.(1983)] Mathewson, D. S., Ford, V. L., Dopita, M. A., Tuohy, I. R., Long, K. S. & Helfand, D. J. 1983, *ApJS*, 51, 345
- [Mills et al.(1982)] Mills, B. Y., Little, A. G., Durdin, J. M., & Kesteven, M. J. 1982, *MNRAS*, 200, 1007
- [Nishiuchi(2001)] Nishiuchi, M. 2001, Ph.D. thesis, Kyoto University
- [Ohashi et al.(1996)] Ohashi, T., Ebisawa, K., Fukazawa, Y., Hiyoshi, K., Horii, M., Ikebe, Y., Ikeda, H., Inoue, H. et al. 1996, *PASJ*, 48, 157
- [Rho, Petre(1998)] Rho, J., & Petre, R. 1998, *ApJ*, 503, L167
- [Rosado et al.(1994)] Rosado, M., Le Coarer, E., & Georgelin, Y. P. 1994, *A&A*, 286, 231
- [Russell, Dopita(1992)] Russell, S. C., & Dopita, M. A. 1992, *ApJ*, 384, 508
- [Serlemitsos et al.(1995)] Serlemitsos, P. J., Jalota, L., Soong, Y., Kunieda, H., Tawara, Y., Tsusaka, Y., Suzuki, H., Sakima, Y. et al. 1995, *PASJ*, 47, 105
- [Shelton(1999)] Shelton, R. L. 1999, *ApJ*, 521, 217
- [Tsujiimoto et al.(1995)] Tsujimoto, T., Nomoto, K., Yoshii, Y., Hashimoto, M., Yanagita, S., & Thielemann, F.-K. 1995, *MNRAS*, 277, 945
- [van den Bergh(2000)] van den Bergh, S. 2000, *PASP*, 112, 529
- [White, Long(1991)] White, R. L., & Long, K. S. 1991, *ApJ*, 373, 543
- [Williams et al.(1999)] Williams, R. M., Chu, Y.-H., Dickel, J. R., Petre, R., Smith, R. C., & Tavaréz, M. 1999, *ApJS*, 123, 467
- [Ye et al.(1991)] Ye, T., Turtle, A. J., & Kennicutt, R. C. Jr., 1991, *MNRAS*, 249, 722
- [Yokogawa et al.(2000)] Yokogawa, J., Imanishi, K., Tsujimoto, M., Nishiuchi, M., Koyama, K., Nagase, F., Corbet, R. H. D. 2000, *ApJS*, 128, 491

**Table 1.** Observation log.

ASCA/SIS			
Target	Date	Exposure (ks)	SIS mode*
0103–726	1996/05/21–23	60.8	1-CCD Faint/Faint
0045–734	1997/11/13–14	37.8	2-CCD Faint/Faint
0057–7226	1997/11/14–15	33.8	2-CCD Faint/Faint
0045–734	2000/04/11–17	95.9	2-CCD Faint/Bright
ROSAT/HRI			
Target	Date	Exposure (ks)	
0045–734	1994/04/17–18	4.4	
0057–7226	1994/04/19–06/09	14.8	
0045–734	1994/04/21–05/16	7.4	
0057–7226	1995/04/13–05/12	34.3	
0103–726	1996/12/13	1.1	
0103–726	1997/03/28–04/14	16.7	
0103–726	1997/04/19–06/12	12.8	

\* Data format in the high/medium bit rate.

**Table 2.** Best-fit parameters for the spectrum of the SNRs.

SNR	0103–726		0045–734		0057–7226
Model*	I	III	I	II	...
$\log \tau$ (s cm <sup>-3</sup> )	10.97 <sup>+0.21</sup> <sub>-0.21</sub>	10.82 <sup>+0.25</sup> <sub>-0.26</sub>	13.00 <sup>§+∞</sup> <sub>-1.20</sub>	11.74 <sup>+∞</sup> <sub>-0.41</sub>	11.01 <sup>+∞</sup> <sub>-0.44</sub>
$kT_e$ (keV)	0.67 <sup>+0.13</sup> <sub>-0.10</sub>	1.0 <sup>+0.5</sup> <sub>-0.2</sub>	0.37 <sup>+0.10</sup> <sub>-0.05</sub>	0.96 <sup>+0.08</sup> <sub>-0.05</sub>	0.9 <sup>+0.8</sup> <sub>-0.3</sub>
$N_H$ (10 <sup>21</sup> H cm <sup>-2</sup> )	0 <sup>+0.5</sup>	0 <sup>+0.3</sup>	10 <sup>+1</sup> <sub>-2</sub>	3 <sup>+1</sup> <sub>-2</sub>	1 <sup>+2</sup> <sub>-1</sub>
Norm <sup>†</sup> (10 <sup>11</sup> cm <sup>-5</sup> )	0.86	0.28	3.9	0.45	0.51
Flux <sup>‡</sup> (erg s <sup>-1</sup> cm <sup>-2</sup> )	1.1 × 10 <sup>-12</sup>	1.0 × 10 <sup>-12</sup>	2.9 × 10 <sup>-13</sup>	3.1 × 10 <sup>-13</sup>	3.0 × 10 <sup>-13</sup>
— Abundances (solar unit) —					
O	0.5 <sup>+0.3</sup> <sub>-0.1</sub>	1.7 <sup>+3.0</sup> <sub>-0.7</sub>	0.2 (fixed)	0.2 (fixed)	0.2 (fixed)
Ne	1.0 <sup>+0.2</sup> <sub>-0.2</sub>	1.9 <sup>+1.7</sup> <sub>-0.6</sub>	2.6 <sup>+1.0</sup> <sub>-0.7</sub>	0.2 (fixed)	0.2 (fixed)
Mg	0.9 <sup>+0.3</sup> <sub>-0.2</sub>	2.0 <sup>+1.8</sup> <sub>-0.8</sub>	1.0 <sup>+0.5</sup> <sub>-0.4</sub>	1.6 <sup>+1.7</sup> <sub>-0.6</sub>	0.2 (fixed)
Si	0.4 <sup>+0.2</sup> <sub>-0.2</sub>	0.7 <sup>+1.1</sup> <sub>-0.4</sub>	0.2 (fixed)	0.2 (fixed)	0.2 (fixed)
Fe	0.2 (fixed)	1.0 <sup>+1.1</sup> <sub>-0.5</sub>	0.2 (fixed)	0.9 <sup>+0.5</sup> <sub>-0.3</sub>	0.2 (fixed)
Reduced $\chi^2$ /d.o.f.	1.47/64	1.41/63	1.45/89	1.60/89	0.91/22

Note. Errors indicate the 90% confidence limits.

\* Defined in subsection 3.2.

† Norm  $\equiv EM/4\pi D^2$ , where  $D$  is the distance (60 kpc) and  $EM$  is the emission measure.

‡ In 0.7–10.0 keV.

§ Pegged by the upper limit of the plasma code.

**Table 3.** Parameters derived from the best-fit models for the SNRs.

SNR Model*	0103–726		0045–734		0057–7226
	I	III	I	II	...
$V$ ( $\beta$ cm <sup>3</sup> )	— $1.3 \times 10^{60}$ —		— $3.6 \times 10^{59}$ —		$6.6 \times 10^{59}$
$n_e$ ( $\beta^{-1/2}$ cm <sup>-3</sup> )	0.17	0.097	0.69	0.23	0.18
$t$ ( $\beta^{1/2}$ yr)	$1.8^{+1.0}_{-0.7} \times 10^4$	$2.2^{+1.6}_{-1.0} \times 10^4$	(> $2.9 \times 10^4$ )	$7.6^{+\infty}_{-4.7} \times 10^4$	$1.8^{+\infty}_{-1.2} \times 10^4$
$M_{\text{total}}$ ( $\beta^{1/2} M_{\odot}$ )	180	110	210	69	100
Element mass ( $\beta^{1/2} M_{\odot}$ )					
O	$5.6^{+3.3}_{-1.1} \times 10^{-1}$	$1.2^{+2.0}_{-0.5}$	... <sup>†</sup>	... <sup>†</sup>	... <sup>†</sup>
Ne	$2.0^{+0.4}_{-0.4} \times 10^{-1}$	$2.3^{+2.1}_{-0.7} \times 10^{-1}$	$6.0^{+2.3}_{-1.6} \times 10^{-1}$	... <sup>†</sup>	... <sup>†</sup>
Mg	$6.7^{+2.3}_{-1.5} \times 10^{-2}$	$9.1^{+7.9}_{-3.6} \times 10^{-2}$	$8.6^{+4.4}_{-3.4} \times 10^{-2}$	$4.6^{+4.9}_{-1.7} \times 10^{-2}$	... <sup>†</sup>
Si	$3.3^{+1.6}_{-1.7} \times 10^{-2}$	$3.5^{+5.5}_{-2.0} \times 10^{-2}$	... <sup>†</sup>	... <sup>†</sup>	... <sup>†</sup>
Fe	... <sup>†</sup>	$1.2^{+1.4}_{-0.6} \times 10^{-1}$	... <sup>†</sup>	$6.9^{+4.1}_{-2.3} \times 10^{-2}$	... <sup>†</sup>

Note. The volume filling factor is represented by  $\beta$ . Errors are derived from the 90% confidence limits for  $\tau$  and elemental abundances in the spectral fitting (table 2).

\* Defined in subsection 3.2.

† Fixed to be 0.2 solar abundance in the spectral fitting.